Activation of Ethane C−H and C−C Bonds by Gas Phase Th^+ and U^+: A Theoretical Study†

E. Di Santo, M. C. Michelini, and N. Russo*

Dipartimento di Chimica and Centro di Calcolo ad Alte Prestazioni per Elaborazioni Parallele e Distribuite-Centro d'Eccellenza MURST, Università della Calabria, I-87030 Arcavacata di Rende, Italy

Received: May 22, 2009; Revised Manuscript Received: August 11, 2009

Two different approaches of density functional theory were used to analyze the C−H and C−C bond activation mechanisms during the reaction of bare Th^+ and U^+ ions with ethane. We report a complete exploration of the potential energy surfaces taking into consideration different spin states. According to B3LYP/SDD computations the double dehydrogenation of C_2H_6 is thermodynamically favorable only in the case of Th^+. It is shown that the overall C−H and C−C bond activation processes are exothermic in the case of Th^+ and endothermic for U^+. In both cases, the C−C insertion transition state barrier exceeds the energy of the ground state reactants, preventing the observation of these species under thermal conditions.

1. Introduction

In the past decade a great body of studies has been performed on the reactivity of actinide cations with small molecules in the gas phase.[1−4] This research has been mainly carried out using mass spectroscopic techniques, which are able to provide thermochemical data as well as some insight into the reaction mechanisms.[1−3] The main goal of these studies has been to analyze the reactivity and bonding of the metal ions, which in the absence of perturbing factors correlate directly with their electronic structures and energetics. In early actinides it is particularly interesting to analyze the possible active role of the 5f electrons in reactivity. Recent theoretical calculations have permitted a detailed description of the reaction mechanisms of activation of small molecules by bare actinide cations.[4]

The activation of C−H and C−C bonds by transition metal (TM) ions in the gas phase has been an active area of research that provides fundamental information on reaction mechanisms, kinetics, and thermodynamics.[5]

A number of experimental and theoretical studies on the reactivity of bare transition-metal ions with methane have provided a wealth of insight concerning the C−H bond activation process.[6−10] Those studies have demonstrated that none of the first- or second-row transition metal ions reacts with methane at thermal energies. In contrast, it was shown that several of the third-row transition metal ions (Ta^+, W^+, Os^+, Ir^+, and Pt^+) react exothermically to dehydrogenate methane.[8−10] In a recent series of papers, Armentrout and co-workers have revisited, both experimentally and theoretically, the reactivity of most of the third-row TMs monocations (Hf^+, Ta^+, W^+, Re^+, Ir^+, Pt^+, and Au^+) with CH_4.[10]

Recent theoretical works[4e,11] have reported the reaction mechanisms of the interaction of actinide monocations with CH_4.

Ethane is the simplest alkane in which both the C−H and C−C bonds can be activated. Detailed experimental and theoretical studies of the reactivity of the first-[12] and second-row[13] transition metal ions with C_2H_6 have given insight into the electronic requirements of the metal for C−H and C−C bond activation. It was reported that the early members of the first-row TM series (Sc^+, Ti^+, and V^+) show no barrier and exhibit large cross sections for dehydrogenation of ethane, whereas for Fe^+, Co^+, and Ni^+ the reaction occurs with substantial activation barriers. For Cr^+, Mn^+, and Cu^+, no reaction is observed. Demethanation is observed only for the 3d metals Sc^+−Cr^+. It was generaly found that the reactivity is highly dependent on the spin state. In particular, in the cases in which the rate-determining step is the insertion of the metal into a C−H or a C−C bond, the electron spin conservation and electronic configuration restrict which reactant states are more active. Low-spin states are usually more efficient due to the spin-allowed reaction. For a recent review on this subject see ref 5e. For earlier reviews see refs 6b, 6d, and 14.

The reactivity of the 4d transition metal cations with C_2H_6 and higher alkanes has been much less studied, and only in a few cases were the reaction mechanisms studied in detail.[13]

The reactivity of thorium cations with alkanes and alkenes has been studied by Marçalo and co-workers using Fourier transform ion cyclotron resonance/mass spectrometry (FTICR-MS).[3a] It was found that Th^+ ions react exothermically with the studied alkanes and alkenes giving single and/or double dehydrogenation. In the particular case of ethane, the reaction leads to single and double dehydrogenation, with formation of $ThC_2H_4^+$ and $ThC_2H_2^+$ in a 1:1 ratio with a moderate efficiency. More recently, the gas-phase reactions of An^+ and AnO^+ ions (An = Th through Cm) with hydrocarbons has been systematically examined using FTICR-MS techniques.[3b] The results obtained for the reaction of Th^+ with C_2H_6 are in agreement with the earlier results obtained by Marçalo and collaborators.[3a] In the case of uranium the efficiency is under the detection limit ($k/k_{COL} \leq 0.001$).[3b]

Determining reaction mechanisms is one of the more challenging problems in computational chemistry. It has been shown that reactions involving gas-phase An^+ ions often involve crossings between surfaces of different spin states,[4] as usually occur in transition metal mediated reations. The idea of state-selective reactivity has been introduced, at first, by Armentrout and co-workers and the role of spin flip in organometallic chemistry has been underlined by the introduction of the so-called Two State Reactivity (TSR) paradigm.[6b,15] In the case of actinide chemistry the formal spin may vary during a reaction

† Part of the "Vincenzo Aquilanti Festschrift".

* Author to whom correspondence should be sent, nrusso@unical.it.

10.1021/jp9048154
Published on Web 09/01/2009

without appreciably affect the rate due to the fact that weak spin−orbit coupling does not apply to the heavy metal ions and the requirement for spin-conservation is thereby relaxed.

In the framework of a more extended project[4] aiming to unravel the mechanistic details of catalytic processes for the activation of prototypical bonds mediated by bare actinide ions, we have analyzed the reaction of thorium and uranium monocations with ethane. Density functional theory (DFT) has been applied to characterize all the intermediates and first-order saddle points and to obtain a complete mechanistic scheme of the reactions.

The reaction mechanisms for the activation of both the C−C and C−H bonds have been studied according to the general scheme proposed for this kind of reaction that involves as the first step the formation of a metal−ligand adduct followed by an oxidative insertion of the metal center into a ligand molecule bond. The formation of the first insertion intermediate is usually the key step of the whole process, and its formation involves often a crossing between different spin surfaces. The next steps are migration of one or more atoms of the ligand molecule to the metal and reductive elimination of a small molecule provided that intermediates have sufficiently high lifetimes to undergo rearrangements. Bond breakings that are generally not accessible at thermal energies become dominant at high energies.

2. Computational Details

We have used two different approaches of DFT to analyze the reactions under study. This choice was made on the base of the performance observed in our previous studies of the bare actinide cations reactivity.[4] First, DFT in its three-parameter hybrid B3LYP[16] formulation was used together with the Stuttgart−Dresden basis set for the uranium atom (25s 16p 15d 7f)/[7s 6p 5d 3f] in combination with the 60 core electrons[17] relativistic effective core potential (RECP). This small-core RECP, so-called SDD pseudopotential, replaces the 60 electrons in the inner shells 1 through 4, leaving the explicit treatment of the $n = 5$ shell (5s 5p 5d and 5f), and also the 6s, 6p, 6d, and 7s valence electrons. The 6-311++G(d,p) basis set of Pople and co-workers was employed for the rest of the atoms[18] (we refer to these results as B3LYP/SDD, hereafter). These calculations were carried out with the GAUSSIAN 2003 package.[19]

Further calculations were done using the ADF2004.01 package.[20] The zero-order regular approximation (ZORA) was employed in ADF calculations. This approximation was used together with the PW91 functionals (exchange and correlation)[21] and triple-ζ (TZ2P) basis sets (PW91/ZORA level, hereafter). We have used the frozen-core approach as implemented in ADF to describe the inner electrons of thorium and uranium. Therefore, for both actinide cations all electrons up to 5d were considered as frozen, the remaining electrons constituted the active valence shell.

Full geometry optimizations were performed at both, B3LYP/SDD and PW91/ZORA levels, trying several initial geometries for each species. The nature of the calculated stationary points was characterized by a vibrational analysis performed within the harmonic approximation. The zero-point vibrational energy corrections were included in all the reported relative energies. We have ensured that every transition state has only one imaginary frequency and that the frequency connects reactants and products by means of IRC (intrinsic reaction coordinate) calculations. Unless otherwise mentioned, all energies and geometrical parameters reported in the next sections refers to the B3LYP/SDD results, whereas in all figures are reported the results obtained at both levels of theory. We have chosen the B3LYP/SDD computations as our reference results, due to the better agreement of these results with the existent experimental data. In section 4 we present a comparison of the results obtained at B3LYP/SDD and PW91/ZORA levels.

3. Results and Discussion

3.1. An^+ (An = Th, U) + C_2H_6: Bare Cations and Reaction Mechanisms. At the B3LYP/SDD level the doublet $[Rn]5f^17s^2$ configuration is the lowest-energy electronic configuration of Th^+, with the quartet $[Rn]6d^27s$ 24 kJ/mol higher in energy, whereas at the PW91/ZORA level of theory the bare Th^+ ground state (GS) has a quartet spin state derived from the $[Rn]6d^27s$ configuration. The GS level of the Th^+ cation is actually not identified in the Blaise and Wyart tables[22] due to a strong multiconfiguration mixing. The ground level has a mixed $^4F-^2D$ character.

According to the Blaise and Wyart tables, the lowest-energy U^+ has a $[Rn]5f^37s^2$ electronic configuration (quartet spin state) and is followed closely by several sextet spin states.[22] In this case, the experimental bare cation levels are better reproduced by B3LYP/SDD computations. The calculated GS has in fact a $[Rn]5f^37s^2$ electronic configuration (quartet state) and is followed by two sextet states very close in energy, $[Rn]5f^36d7s$ at around 6 kJ/mol and the $[Rn]5f^47s$ state at 17 kJ/mol, whereas the $[Rn]5f^37s^2$ doublet spin state is much higher in energy (around 71 kJ/mol over the quartet GS). At the PW91/ZORA level the computed GS has a $[Rn]5f^47s$ (sextet) configuration, whereas the $[Rn]5f^37s^2$ (quartet) was found at 55 kJ/mol over the GS. The details of the calculated bare cations energy gaps have been reported elsewhere.[4a,c,e]

In our calculations we have explored the first and second dehydrogenation and the demethanation of C_2H_6 by bare Th^+ and U^+ cations. The activation of the first C−H bond yields to the formation of $AnC_2H_4^+$ (An = Th, U) with the release of one H_2 molecule, whereas the activation of the C−C bond yields to the formation of the methylidene complex, $AnCH_2^+$, and CH_4. The second dehydrogenation reaction, which starts with the reaction product of the first H_2 elimination, $AnC_2H_4^+$, involves the activation of two C−H bonds and leads to the formation of $AnC_2H_2^+$.

As in the case of the activation of alkanes by transition metal cations,[12,13] the proposed mechanisms involve an initial oxidative mechanism in which the cation An^+ inserts in the C−H or C−C bond to form a first insertion intermediate $C_2H_5-An^+-H$ or $CH_3-An^+-CH_3$. The reaction products can then be formed by reductive elimination of small molecules such as H_2 and CH_4 or by metal−hydrogen or metal−carbon bond cleavage, which usually takes place at high energies. From the $C_2H_5-An^+-H$ intermediate the dehydrogenation process evolves through the formation of a dihydride intermediate, $(H)_2An^+-C_2H_4$, which reductively eliminates H_2. The reaction mechanism involves the formation of a third intermediate, $(H_2)An^+-C_2H_4$ in which the H_2 molecule is already formed and prepared for the elimination. In contrast, the demethanation process involves only two transition states, the first one that yields to the formation of the previously mentioned dimethyl intermediate, $CH_3-An^+-CH_3$, and a second transition state that involves the transfer of an H atom between the methyl groups, to form the final adduct $(CH_4)An^+-CH_2$. We note that in most of the reaction pathways reported for the C−H bond activation of C_2H_6 by TM cations, the reaction mechanism does not involve a β-hydrogen shift resulting in dihydrido intermediates. Instead, the reactions usually proceed through a concerted saddle point connecting the C−H inserted species directly with a complex of the TM cation with molecular hydrogen and ethylene.

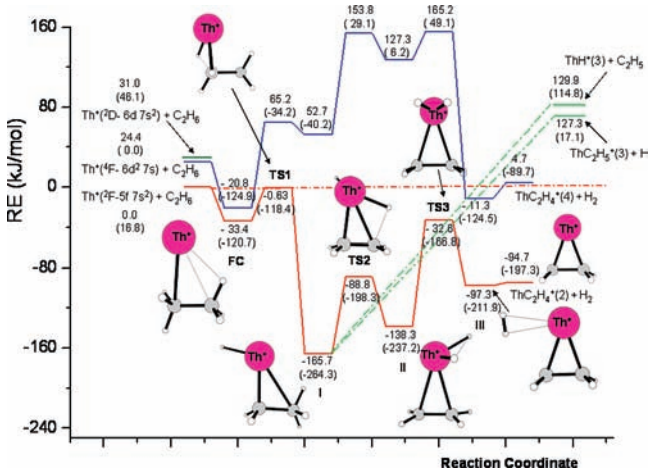

Figure 1. B3LYP/SDD (PW91/ZORA) quartet and doublet PESs for the first dehydrogenation of C_2H_6 by Th^+. Energies are in kJ/mol and relative to the ground-state reactants.

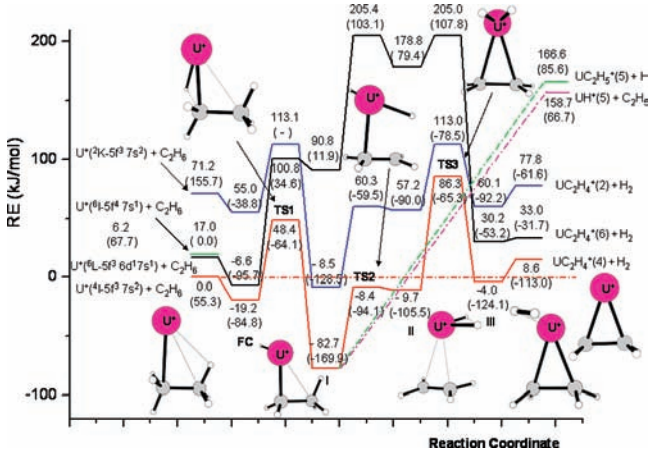

Figure 2. B3LYP/SDD (PW91/ZORA) quartet, sextet, and doublet PESs for the first dehydrogenation of C_2H_6 by U^+. Energies are in kJ/mol and relative to the ground-state reactants.

The second dehydrogenation reaction starts with the $AnC_2H_4^+$ adduct and as in the case of the first dehydrogenation reaction involves three transition states. The first one leads to the formation of the $C_2H_3-An^+-H$ intermediate, which after surpassing the second transition state yields a dihydride intermediate, $(H)_2An^+-C_2H_2$. Then the system evolves to the dehydrogenation products through the formation of the last insertion intermediate, $(H_2)An^+$-C_2H_2, which is basically formed from two moieties, H_2 and $An^+-C_2H_2$.

3.2. C−H Bond Activation: Formation of $ThC_2H_4^+ + H_2$ and $UC_2H_4^+ + H_2$. We will begin by discussing the interaction of An^+ (An = Th, U) cations with the C−H bond in ethane. As shown in Figures 1 and 2, the first step of the dehydrogenation reaction of ethane by bare An^+ cations is the exothermic formation of an $An(C_2H_6)^+$ complex. According to B3LYP/SDD results the reaction of $Th^+ + C_2H_6$ evolves completely along the doublet spin state, whereas at PW91/ZORA level we found that the doublet and quartet $Th(C_2H_6)^+$ structures are almost degenerate in energy, with the quartet state slightly favored. As discussed in the previous section (see also ref 4e), B3LYP/SDD and PW91/ZORA levels do not agree in the ordering of the Th^+ atomic states, and this is reflected also in the stability ordering of the initial complexes. However, both levels of theory agree in that the quartet spin surface becomes very high in energy throughout the rest of the PEP.

In the case of U^+ the reaction evolves completely along the quartet bare cation ground state (B3LYP/SDD). As explained below, at PW91/ZORA there is a double crossing between the doublet and quartet spin surfaces at the stage of the last transition state. The geometrical parameters corresponding to all the species involved in the reaction pathways at both studied levels of theory are reported as Supporting Information (Figures S1 and S2, respectively).

The reaction proceeds to form the first insertion intermediate $H-An^+-C_2H_5$ through the first-order saddle point **TS1** in which the cations are inserted into one of the C−H bonds. The imaginary frequencies ($1051i$ cm^{-1} for Th and $1222i$ cm^{-1} for U), correspond to the C−H bond breaking. In both studied reactions this intermediate (**I**) is the global minimum of the potential energy profile and lies at −165.7 kJ/ml below the ground state reactants in the Th^+ reaction and at −82.7 kJ/mol in the U^+ reaction. The H−An bond distance is very close to the same distance in the corresponding hydrides: ThH^+ ($^3\Delta$, 1.99 Å) and UH^+ ($^5\Delta$, 1.97 Å).

Following the C−H bond insertion, the reaction proceeds through a second intramolecular rearrangement to yield a new intermediate, which can be described as a covalently bonded dihydrido complex, $(H)_2An^+-C_2H_4$, obtained by a hydrogen transfer from the second carbon atom to the metal center. In this complex the H−An bond distances are also very close to the corresponding values in the cationic hydrides (see Figures S1 and S2 in Supporting Information). These intermediates are formed after the system surpasses the second transition state, **TS2**, which are characterized by imaginary frequencies (768i cm^{-1} for Th^+ and 340i cm^{-1} for U^+) that involve the stretching of the C−H bond that is being broken. The lower stability of the second insertion intermediate (**II**) with respect to the first insertion intermediate (**I**) can be understood considering that Th^+ in its doublet spin state has only two electrons available for bonding; therefore, the transfer of the second H atom to form the dihydrido intermediate provokes a lengthening of the $Th^+-(C_2H_4)$ distances (2.58 and 2.64 Å, see Figure S1in Supporting Information). These distances are shortened after the H_2 molecule is formed (2.29 and 2.33 Å). U^+ in the quartet spin state is able to use two of its valence electrons to form bonds; therefore, the formation of the second insertion intermediate involves the same type of difficulties as the Th^+ species. As can be seen in Figure S2 (Supporting Information) the intermediate **II** in the quartet spin state is formed basically by two moieties, UH_2^+ and C_2H_4, which are about 3 Å. The C_2H_4 fragment is practically undistorted with respect to the equilibrium structure in the free molecule (the C−C distance of free C_2H_4 at the studied levels of theory is 1.33 Å). At this stage of the reaction the doublet spin state is quite low in energy, particularly at the PW91/ZORA level, but not enough to became the GS of this species. We note that for the **TS3** structure, the B3LYP/SDD and PW91/ZORA level of theory do not agree in the assignment of the ground spin state, as B3LYP/SDD favors the quartet state whereas PW91/ZORA indicates the doublet **TS3** structure as the GS. The surmised crossing between the doublet and quartet surfaces would be restricted exclusively to the **TS3** structure, as both levels of theory agree in that once the H_2 molecule is formed, the quartet spin state is clearly lower in energy.

The final intermediate, $(H_2)An^+-C_2H_4$, is formed after the last transition state is surmounted, **TS3**. In this structure the H−H distances are 1.25 (Th) and 1.13 Å (U), respectively. The imaginary frequencies are $1486i$ cm^{-1} in the case of Th^+ and $1169i$ cm^{-1} for U^+ and correspond to the expected H−H

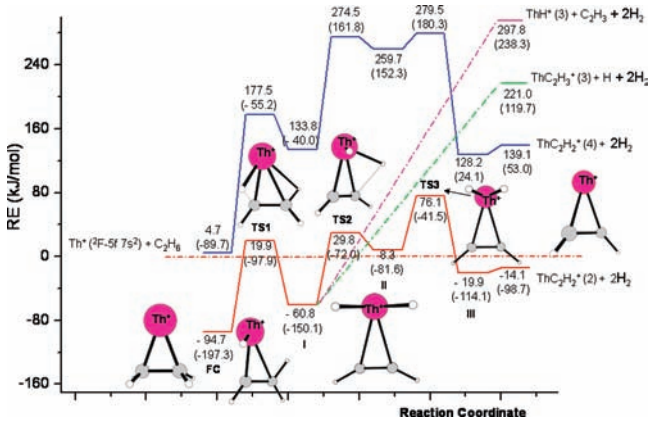

Figure 3. B3LYP/SDD (PW91/ZORA) quartet and doublet PESs for the second dehydrogenation of C_2H_6 by Th^+. Energies are in kJ/mol and relative to the ground-state reactants.

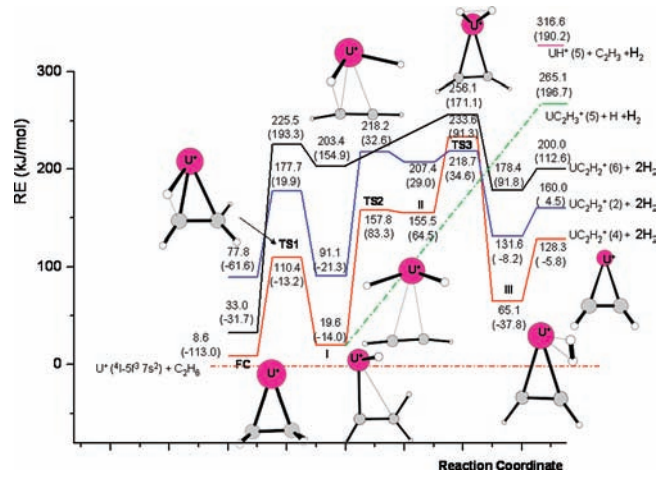

Figure 4. B3LYP/SDD (PW91/ZORA) quartet, sextet, and doublet PESs for the second dehydrogenation of C_2H_6 by U^+. Energies are in kJ/mol and relative to the ground-state reactants.

stretching that yields to the formation of H_2. In the last $(H_2)An^+-C_2H_4$ complex, the hydrogen molecule is already formed and electrostatically interacting between the cationic actinide−ethylene complex.

From the last intermediate, $(H_2)An^+-C_2H_4$, the hydrogen release is endothermic by about 3 kJ/mol in the case of Th^+ and 12.6 kJ/mol for U^+. The overall process is exothermic by about 95 kJ/mol for the reaction of Th^+ and endothermic by almost 9 kJ/mol for U^+.

Different alternative products were also analyzed. In particular, the $H-An^+-C_2H_5$ intermediate is an obvious choice for the formation of AnH^+ and $AnC_2H_5^+$ fragments that can be obtained by simple An−C and An−H bond breaking. Figure 1 shows that the formation of $ThC_2H_5^+$ (^3A) + H is endothermic by around 127 kJ/mol and the production of ThH^+ ($^3\Delta$) is endothermic by almost 130 kJ/mol. In the case of $U^+ + C_2H_6$ the endothermicity is slightly higher, in particular 158.7 kJ/mol (UH^+, $^5\Delta$) and 166.6 kJ/mol ($UC_2H_5^+$,^5A), respectively. The dehydrogenation of C_2H_6 by Th^+ involves transition barriers that in all cases lie below the reactants asymptote, so that the dehydrogenation process could dominate even at high kinetic energies. For U^+, B3LYP/SDD computations indicate that the first and the third reaction barriers are well over the limit represented by the reactants (48.4 and 86.3 kJ/mol, respectively).

3.3. Second Dehydrogenation: Formation of $ThC_2H_2^+ + H_2$ and $UC_2H_2^+ + H_2$. Spontaneous double dehydrogenation was experimentally observed in the reaction of $Th^+ + C_2H_6$;[3] therefore, we have also investigated the reaction mechanisms for the second dehydrogenation process, which yields $AnC_2H_2^+ + H_2$.

The reaction pathways for the second dehydrogenation start from the $AnC_2H_4^+$ reaction products of the first dehydrogenation. As for the first dehydrogenation, the reaction pathways to yield $AnC_2H_2^+ + H_2$ involve a three-step mechanism, which implies the surpassing of three transition states. For simplicity we present the reaction paths for the second elimination in separate pictures, Figures 3 and 4, for the reactions of Th^+ and U^+, respectively. As shown in those figures, the relative energies are calculated with respect to the $An^+ + C_2H_6$ GS reactants. The optimized geometries of all of the key minima and transition states involved in the second H_2 elimination are presented in Figures S3 and S4 (Supporting Information). The imaginary frequencies that characterize all of the transition states at both levels of theory are reported in the same figures.

The isomerization of the initial An^+−ethene adduct to the first insertion intermediate, $H-An^+-C_2H_3$, involves surpassing a transition structure in which one of the C−H bonds is elongated to about 1.6 Å, in both studied reactions. The imaginary vectors involve the elongation of this bond as well as the rotation of the C_2H_4 molecule, to approach to the planar structure that characterizes the $AnC_2H_3^+$ moiety in the following hydrate intermediate (see Figures S3 and S4 in Supporting Information). Along the reaction coordinate we found another transition state that involves the transfer of a second H atom that yields to the formation of a dihydride intermediate (**II**), $(H)_2An^+C_2H_2$, in which the metal−hydrogen distances are very close to 2.0 Å. From this intermediate the reaction evolves to the final $(H_2)An^+C_2H_2$ intermediate, through the surpassing of the last transition state, which is characterized by an imaginary frequency that involves the stretching of the H−H bond. For the same reasons stated in the previous section, also in this case the second insertion intermediate is destabilized with respect to the previous intermediate. In the case of the $U^+ + C_2H_6$ reaction the used levels of theory disagree in the assignation of the ground spin state for the **TS2** and the second intermediate (**II**). Also in this case the PW91/ZORA level favors the doublet spin state, whereas at the B3LYP/SDD level, the quartet spin state is the GS for these species. In summary, for Th^+ the second dehydrogenation evolves completely along the doublet spin surface, whereas in the case of U^+ the reaction evolves mostly on the quartet bare cation ground state, with a double crossing between the doublet and quartet spin surfaces. At the B3LYP/SDD level of theory the crossing takes place around the **TS3** structure, whereas according to the PW91/ZORA level the doublet spin surface is the GS from the formation of the first insertion intermediate (**I**) to the surpassing of **TS3**. Both levels of theory, however, agree that after the surpassing of the last transition state, the reaction evolves completely around the quartet state.

In contrast to the first dehydrogenation reaction, in both Th^+ and U^+ second dehydrogenation reactions, the intrinsic transition barriers associated with the breaking of the two C−H bonds are notably higher than the last one, associated to the formation of the H_2 molecule (see Table 1). The most notable difference between the cations is the higher intrinsic barrier for the second transition state for the reaction of U^+.

We must underline that all the barriers corresponding to the second dehydrogenation reaction are over the limit represented by the $An^+ + C_2H_6$ reactants. However, the relative energy of the barriers is quite low for Th^+. The whole $Th^+ + C_2H_6$ =

TABLE 1: Activation Barriers, in kJ mol^{-1}, of the Transition States Calculated at the B3LYP/SDD (PW91/ZORA) Level

$Th^+ + C_2H_6$	first dehydrogenation	second dehydrogenation	C−C bond activation
TS1[a]	32.8 (2.4)	114.6 (99.4)	105.5 (76.0)
TS2[b]	76.9 (66.0)	90.6 (78.0)	161.5 (126.5)
TS3[c]	105.7 (70.4)	67.8 (40.1)	
$U^+ + C_2H_6$	first dehydrogenation	second dehydrogenation	C−C bond activation
TS1[a]	67.6 (20.7)	101.8 (99.8)	124.5 (73.5)
TS2[b]	74.3 (75.8)	138.2 (53.9)	145.0 (70.4)
TS3[c]	96.0 (40.1)	63.2 (5.6)	

[a] Calculated as the energetic difference between the first transition state (TS1) and the first complex (FC), considering the GS species at each level of theory. [b] Calculated as the energetic difference between the second transition state (TS2) and the first intermediate (I), considering the GS species at each level of theory. [c] Calculated as the energetic difference between the third transition state (TS3) and the second intermediate (II), considering the GS species at each level of theory.

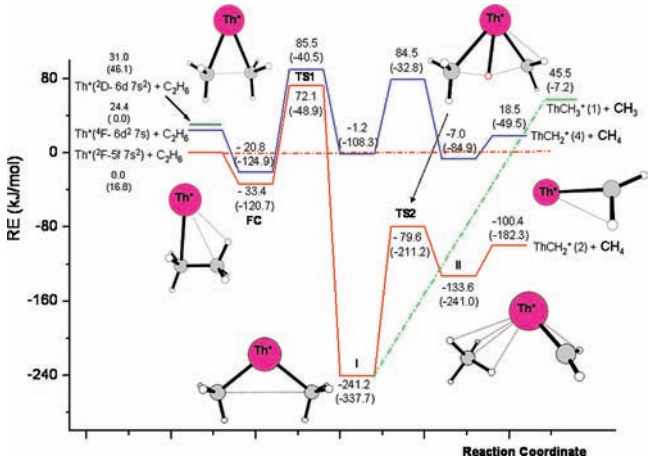

Figure 5. B3LYP/SDD (PW91/ZORA) quartet and doublet PESs for the C−C activation branch of the reaction of Th^+ with C_2H_6. Energies are in kJ/mol and relative to the ground-state reactants.

$ThC_2H_2^+ + 2H_2$ has an exothermicity of 14.1 kJ/mol, whereas the corresponding value for the reaction of U^+ is endothermic by 128.3 kJ/mol (B3LYP/SDD results).

3.4. C−C Bond Activation: Formation of $ThCH_2^+ + CH_4$ and $UCH_2^+ + CH_4$. The PES along the C−C bond activation branch of the $Th^+ + C_2H_6$ and $U^+ + C_2H_6$ reactions are displayed in Figures 5 and 6, respectively, while the corresponding geometrical structures are collected in Figures S5 and S6 (Supporting Information). As shown in Figures 5 and 6 (see also Figures 1 and 2), the initial $An(C_2H_6)^+$ complex is common to both dissociation channels (H_2 and CH_4 elimination). The adduct complex then rearranges to a dimethyl species (**I**), $CH_3-An^+-CH_3$, in which the cations are inserted into the C−C bond. This intermediate is the global minima of the potential energy profiles in both Th^+ and U^+ reactions. For the reaction of $Th^+ + C_2H_6$ the first transition state in its doublet ground spin state is located at around 72 kJ/mol (B3LYP/SDD) over the $Th^+(^2F) + C_2H_6$ asymptote and is characterized by one imaginary frequency of 575*i* cm^{-1}, corresponding to the C−C bond breaking and rotation of one of the CH_3 groups. The quartet and sextet spin state **TS1** structures are almost degenerate in energy (+108.5 and +105.3 kJ/mol) for the $U^+ + C_2H_6$ reaction (see Figure 6). The C−C distance is elongated to 1.93

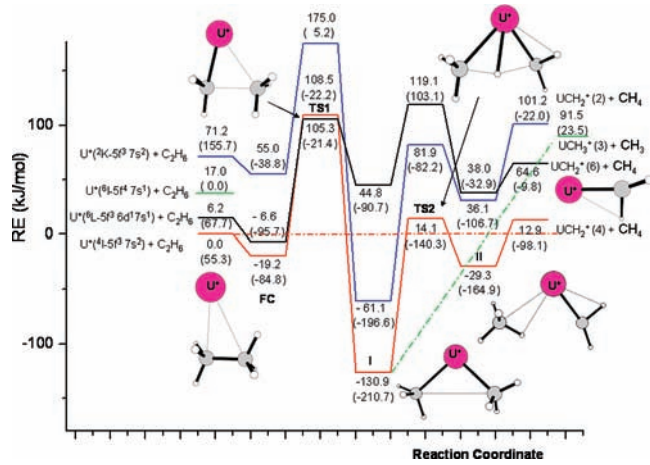

Figure 6. B3LYP/SDD (PW91/ZORA) quartet, sextet, and doublet PESs for the C−C activation branch of the reaction of U^+ with C_2H_6. Energies are in kJ/mol and relative to the ground-state reactants.

Å in Th^+ **TS1** and 2.07 Å in U^+ **TS1**. The formation of the inserted dimethyl intermediate (**I**) is a very exothermic process in both studied reactions and involves a very high energy barrier.

Proceeding along the reaction coordinate, the intermediate (**I**) is converted into another stable ion−molecule complex, $(CH_4)An^+-CH_2$, which serves as the direct precursor for loss of methane. In these intermediates the methane moiety has a distorted η^3 coordination to the metal cation with one of the An^+-H distances quite shorter than the other two. The metal carbon distance is 2.88 Å (B3LYP/SDD) in $(CH_4)-ThCH_2^+$ and 2.77 Å in $(CH_4)-UCH_2^+$. In both structures the metal−methylidene distance is very close to the corresponding value in the carbene cation, 2.04 Å. The structures of the last intermediate (**II**) are characterized by the presence of agostic geometries. In this intermediate the $An^+{=}CH_2$ moieties are very close to the final $AnCH_2^+$ products. The bonding characteristics of the $An^+{=}CH_2$ structures have been discussed elsewhere.[4e] The doublet ground state $(CH_4)Th^+{=}CH_2$ complex is calculated to lie 133.6 kJ/mol below the reactants dissociation limit, while formation of the corresponding uranium species is calculated to be 29.3 kJ/mol.

The saddle point for the 1,3 hydrogen shift that directly converts the dimethyl complex into the $(CH_4)An^+{=}CH_2$ cation (**TS2**) is characterized by an imaginary frequency of 1345*i* cm^{-1} in the case of Th^+ and 1314*i* cm^{-1} for U^+ (B3LYP/SDD). The transition vector associated to these frequencies and the geometries of the transition structures are completely consistent with the 1,3 H-shift, which leads to the final complex (**II**). The relative energy of **TS2** with respect to the reactants is −79.6 kJ/mol (Th^+) and 14.0 kJ/mol (U^+). The structure of this transition state shows one of the An−C distances elongated by about 0.4 Å, while the carbene structure is almost formed. It must be noted that in **TS2** the metal atom participates to some extent to the hydrogen migration as implied by the short An−H distance (2.08 and 2.05 Å for the Th^+ and U^+ **TS2** structures, respectively).

The reductive elimination of methane from the last insertion intermediate, with formation of $An{=}CH_2^+$ is endothermic by around 33 kJ/mol for Th^+ and 42 kJ/mol for U^+. The whole demethanation process is exothermic by around 100 kJ/mol for the $Th^+ + C_2H_6$ reaction and endothermic by almost 13 kJ/mol for $U^+ + C_2H_6$.

From the $CH_3-An^+-CH_3$ intermediate the $AnCH_3^+ + CH_3$ products can be obtained through direct bond cleavage of one

of the An−C bonds. Figures 5 and 6 show that this process is endothermic by 45.5 kJ/mol (Th^+) and 91.5 kJ/mol (U^+), respectively. Direct formation of $AnCH_3^+ + CH_3$ products is, therefore, energetically much more demanding than the tight **TS2** transition state for the 1,3 hydrogen shift.

The first transition state, **TS1**, is by far the most demanding point in the mechanistic scheme for the C−C bond activation, lying 72.1 and 105.3 kJ/mol above the $Th^+ + C_2H_6$ and $U^+ + C_2H_6$ reactants asymptotes, respectively. We conclude, therefore that the lacking of CH_4 elimination in the experiments is due to a kinetic impedance in the case of the $Th^+ + C_2H_6$ reaction, whereas for U^+ the reaction is unfavorable both thermodynamically and kinetically.

4. Comparison between the Different Levels of Theory

As reported in previous theoretical works,[4] a comparison of the relative energies calculated at the two different levels of theory used in this work, B3LYP/SDD and PW91/ZORA, indicates important differences that can be as high as 130 kJ/mol for the GS species of the $Th^+ + C_2H_6$ reaction and 185 kJ/mol in the case of the GS species of the $U^+ + C_2H_6$ reaction. This trend has been previously analyzed, and it was concluded that a significant part of the energy difference is due to the different functionals used in each approach.[4a,b]

In order to give further insight into the origin of these differences, we have recalculated the potential energy surfaces presented in Figures 1−6, using as the asymptote the reaction products in their corresponding ground states, instead of the reactants. The results are presented in Figures S7 to S12 (Supporting Information). It can be seen that the relative energies of the different species calculated at both levels of theory are now much closer, being the greater difference of 39 kJ/mol for the $Th^+ + C_2H_6$ reaction and 120 kJ/mol for the $U^+ + C_2H_6$ reaction. The largest difference between the relative energies calculated at the different levels of theory is now restricted to the relative energy of the $An^+ + C_2H_6$ reactants with respect to the new asymptotes (reaction products in their GSs).

These results seem to indicate that the main reason for the large difference between the relative energies calculated at the B3LYP/SDD and PW91/ZORA levels is the choice of the $An^+ + C_2H_6$ asymptote. We note that the formal oxidation numbers for all the Th^+ species from the formation of the first transition state in the case of the first dehydrogenation (and the C−C bond activation) and for all the species involved in the second dehydrogenation is III. The improvement in the agreement between the B3LYP/SDD and the PW91/ZORA relative energies when considering the reaction products as the reference energy can be considered as an indication of the difficulties of DFT to describe the energetics of reactions that involve important changes in the oxidation states. The same reasoning can be applied the to $U^+ + C_2H_6$ reaction, for which all the species in the first dehydrogenation paths as well as the C−C bond activation process have the same formal oxidation number (III) from the formation of the first transition state. Previous theoretical studies have underlined the shortcomings of DFT to describe quantitatively the energetics of reactions involving changes in the formal oxidation numbers.[23]

5. Summary and Conclusions

The following major conclusions can be inferred from the detailed exploration of the PES for the reaction of Th^+ and U^+ with C_2H_6.

Both hydrogen and methane elimination reactions start with the formation of the $An(C_2H_6)^+$ ion−molecule complex. According to B3LYP/SDD results, the dehydrogenation of C_2H_6 evolves completely along the doublet spin surface. The first H_2 elimination reaction is exothermic by almost 95 kJ/mol and the highest energy point en route to the products is the first C−H insertion transition state that has been located 0.6 kJ/mol below the asymptote represented by the reactants. At the same level of theory the $U^+ + C_2H_6$ reaction proceeds along the quartet U^+ ground state, and the reaction is slightly endothermic (8.6 kJ/mol). The transition barriers associated to the first and third transition states are quite high in energy, well above the $U^+ + C_2H_6$ reactant asymptotes. In both reactions, the direct bond breaking processes from the common intermediate $H-An^+-C_2H_5$ to obtain AnH^+ and $AnC_2H_5^+$ fragments are not energetically competitive. These results indicate, therefore, that the dehydrogenation of C_2H_6 by U^+ in the gas phase is thermodynamically unfavorable, which justifies the nondetection of dehydrogenation during FTICR-MS experiments.

According to B3LYP/SDD computations, the overall methane elimination reaction is predicted to be exothermic by 100 kJ/mol for the activation by Th^+ and endothermic by almost 13 kJ/mol in the case of U^+. Even when the C−C insertion $CH_3-An^+-CH_3$ product is a very stable intermediate, the associated TS barrier is quite large and exceeds the energy of the ground state reactants by 72.1 (Th^+) and 105.3 kJ/mol (U^+), preventing the observation of these species under thermal conditions.

Alternative fragmentation pathways produced by direct bond cleavage appear to become competitive only at significantly higher kinetic energies.

Acknowledgment. Financial support from the Università degli Studi della Calabria and MIUR is gratefully acknowledged.

Supporting Information Available: Optimized geometries of all the intermediates and transition states reported in Figures 1−6 and reaction pathways 1−6 computed considering the GS reaction products as asymptotes to calculate the relative energies. This material is available free of charge via the Internet at http://pubs.acs.org.

References and Notes

(1) (a) Gibson, J. K. *Int. J. Mass Spectrom.* **2002**, *214*, 1. (b) Gibson, J. K.; Marçalo, J. *Coord. Chem. Rev.* **2006**, *250*, 776.

(2) (a) Heinemann, C.; Cornehl, H. H.; Schwarz, H. *J. Organomet. Chem.* **1995**, *501*, 201. (b) Cornehl, H. H.; Heinemann, C.; Marçalo, J.; Pires de Matos, A.; Schwarz, H. *Angew. Chem., Int. Ed. Engl.* **1996**, *35*, 891. (c) Cornehl, H. H.; Wesendrup, R.; Diefenbach, M.; Schwarz, H. *Chem.−Eur. J.* **1997**, *3*, 1083. (d) Santos, M.; Marçalo, J.; Pires de Matos, A.; Gibson, J. K.; Haire, R. G. *J. Phys. Chem. A* **2002**, *106*, 7190. (e) Santos, M.; Marçalo, J.; Leal, J. P.; Pires de Matos, A.; Gibson, J. K.; Haire, R. G. *Int. J. Mass Spectrom.* **2003**, *228*, 457. (f) Gibson, J. K.; Haire, R. G.; Santos, M.; Marçalo, J.; Pires de Matos, A. *J. Phys. Chem. A* **2005**, *109*, 2768.

(3) (a) Marçalo, J.; Leal, J. P.; Pires de Matos, A. *Int. J. Mass Spectrom. Ion Processes* **1996**, *157/158*, 265. (b) Gibson, J. K.; Haire, R. G.; Marçalo, J.; Santos, M.; Pires de Matos, A.; Mrozik, M. K.; Pitzer, R. M.; Bursten, B. E. *Organometallics* **2007**, *26*, 3947.

(4) (a) Michelini, M. C.; Russo, N.; Sicilia, E. *Angew. Chem., Int. Ed.* **2006**, *45*, 1095. (b) Michelini, M. C.; Russo, N.; Sicilia, E. *J. Am. Chem. Soc.* **2007**, *129*, 4229. (c) Mazzone, G.; Michelini, M. C.; Russo, N.; Sicilia, E. *Inorg. Chem.* **2008**, *47*, 2083. (d) Alikhani, M. E.; Michelini, M. C.; Russo, N.; Silvi, B. *J. Phys. Chem. A* **2008**, *112*, 12966. (e) Di Santo, E.; Michelini, M. C.; Russo, N. *Organometallics* **2009**, *28*, 3716.

(5) (a) Arakawa, H.; Aresta, M.; Armor, J. N.; Barteau, M. A.; Beckman, E. J.; Bell, A. T.; Bercaw, J. E.; Creutz, C.; Dinjus, E.; Dixon, D. A.; Domen, K.; DuBois, D. L.; Eckert, J.; Fujita, E.; Gibson, D. H.; Goddard, W. A.; Goodman, D. W.; Keller, J.; Kubas, G. J.; Kung, H. H.; Lyons, J. E.; Manzer, L. E.; Marks, T. J.; Morokuma, K.; Nicholas, K. M.; Periana, R.; Que, L.; Rostrup-Nielson, J.; Sachtler, W. M. H.; Schmidt, L. D.; Sen, A.; Somorjai, G. A.; Stair, P. C.; Stults, B. R.; Tumas, W. *Chem. Rev.* **2001**, *101*, 953. (b) Crabtree, R. H. *J. Chem. Soc., Dalton Trans.*

2001, 2437. (c) Labinger, J. A.; Bercaw, J. E. *Nature* **2002**, *417*, 507. (d) Bergman, R. G. *Nature* **2007**, *446*, 391. (e) Schwarz, H. *Int. J. Mass Spectrom.* **2004**, *237*, 75. (f) Schröder, D.; Schwarz, H. *Proc. Natl. Acad. Sci. U.S.A.* **2008**, *105*, 18114.

(6) See for instance: (a) Tolbert, M. A.; Beauchamp, J. L. B. *J. Am. Chem. Soc.* **1984**, *106*, 8117. (b) Armentrout, P. B.; Beauchamp, J. L. *Acc. Chem. Res.* **1989**, *22*, 315. (c) Armentrout, P. B. *Sience* **1991**, *251*, 175. (d) Weisshaar, J. C. *Acc. Chem. Res.* **1993**, *26*, 213. (e) Liu, F.; Zhang, X.-G.; Armentrout, P. B. *Phys. Chem. Chem. Phys.* **2005**, *7*, 1054.

(7) See for instance: (a) Russo, N.; Sicilia, E. *J. Am. Chem. Soc.* **2001**, *123*, 2588. (b) Sicilia, E.; Russo, N. *J. Am. Chem. Soc.* **2002**, *124*, 1471. (c) Michelini, M. C.; Russo, N.; Sicilia, E. *J. Phys. Chem. A* **2002**, *106*, 8937. (d) Michelini, M. C.; Sicilia, E.; Russo, N.; Alikhani, M. E.; Silvi, B. *J. Phys. Chem. A* **2003**, *107*, 4862. (e) Chiodo, S.; Kondakova, O.; Michelini, M. C.; Russo, N.; Sicilia, E. *J. Phys. Chem. A* **2004**, *108*, 1069.

(8) (a) Irikura, K. K.; Beauchamp, J. L. *J. Am. Chem. Soc.* **1989**, *111*, 75. (b) Irikura, K. K.; Beauchamp, J. L. *J. Am. Chem. Soc.* **1991**, *113*, 2769. (c) Irikura, K. K.; Beauchamp, J. L. *J. Phys. Chem.* **1991**, *95*, 8344. (d) Irikura, K. K.; Goddard, W. A., III. *J. Am. Chem. Soc.* **1994**, *116*, 8733.

(9) (a) Buckner, S. W.; MacMahon, T. J.; Byrd, G. D. B. S. *Inorg. Chem.* **1989**, *28*, 3511. (b) Ranasinghe, Y. A.; MacMahon, T. J.; Freiser, B. S. *J. Phys. Chem.* **1991**, *95*, 7721. (c) Blomberg, M. R. A.; Siegbahn, P. E. M.; Svensson, M. *J. Phys. Chem.* **1994**, *98*, 2062. (d) Perry, J. K.; Ohanessian, G.; Goddard, W. A., III. *Organometallics* **1994**, *13*, 1870. (e) Wesendrup, R.; Schröeder, D.; Schwarz, H. *Angew. Chem., Int. Ed.* **1994**, *33*, 1174. (f) Irikura, K. K.; Goddard, W. A., III. *J. Am. Chem. Soc.* **1994**, *116*, 8733. (g) Heinemann, C.; Hertwig, R. H.; Wesendrup, R.; Koch, W.; Schwarz, H. *J. Am. Chem. Soc.* **1995**, *117*, 495. (h) Pavlov, M.; Blomberg, M. R. A.; Siegbahn, P. E. M. *J. Phys. Chem. A* **1997**, *101*, 1567. (i) Heinemann, C.; Schwarz, H.; Koch, W.; Dyall, K. *Chem. Phys.* **1996**, *104*, 4642. (j) Heinemann, C.; Wesendrup, R.; Schwarz, H. *Chem. Phys. Lett.* **1995**, *239*, 75. (k) Achatz, U.; Beyer, M.; Joos, S.; Fox, B. S.; Nieder-Schatteburg, G.; Bondybey, V. E. *J. Phys. Chem. A* **1999**, *103*, 8200. (l) Heinemann, C.; Koch, W.; Schwarz, H. *Chem. Phys. Lett.* **1995**, *245*, 509. (m) Holthausen, M. C.; Heinemann, C.; Cornehl, H. H.; Koch, W.; Schwarz, H. *J. Chem. Phys.* **1995**, *102*, 4931.

(10) (a) Zhang, X.-G.; Liyanage, R.; Armentrout, P. B. *J. Am. Chem. Soc.* **2001**, *123*, 5563. (b) Armentrout, M. M.; Li, F.-X.; Armentrout, P. B. *J. Phys. Chem. A* **2004**, *108*, 9660. (c) Parke, L. G.; Hinton, C. S.; Armentrout, P. B. *Int. J. Mass Spectrom.* **2006**, *254*, 168. (d) Li, F.-X.; Armentrout, P. B. *J. Chem. Phys.* **2006**, *125*, 133114. (e) Armentrout, P. B.; Shin, S.; Liyanage, R. *J. Phys. Chem. A* **2006**, *110*, 1242. (f) Li, F.-X.; Zhang, X.-G.; Armentrout, P. B. *Int. J. Mass Spectrom.* **2006**, *255*−*256*, 279. (g) Parke, L. G.; Hinton, C. S.; Armentrout, P. B. *J. Phys. Chem. C* **2007**, *111*, 17773.

(11) De Almeida, K. J.; Duarte, H. A. *Organometallics* **2009**, *28*, 3203.

(12) (a) Sanders, L.; Hanton, S. D.; Weisshaar, J. C. *J. Phys. Chem.* **1987**, *91*, 5145. (b) Sanders, L.; Hanton, S. D.; Weisshaar, J. C. *J. Chem. Phys.* **1990**, *92*, 3498. (c) Holthausen, M. C.; Fiedler, A.; Koch, W.; Schwarz, H. *Angew. Chem., Int. Ed. Engl.* **1995**, *34*, 2282. (d) Holthausen, M. C.; Koch, W. *J. Am. Chem. Soc.* **1996**, *118*, 9932. (e) Holthausen, M. C.; Fiedler, A.; Koch, W.; Schwarz, H. *J. Phys. Chem.* **1996**, *100*, 6236. (f) Sievers, M. R.; Chen, Y.-M.; Haynes, C. L.; Armentrout, P. B. *Int. J. Mass Spectrom.* **2000**, *195/196*, 149. (g) Zhang, D.; Liu, C.; Bi, S.; Yuan, S. *Chem.—Eur. J.* **2003**, *9*, 484. (h) Zhang, D.; Liu, C.; Wensheng, B. *J. Mol. Struct.: THEOCHEM* **2003**, *635*, 239.

(13) (a) Chen, Y.-M.; Armentrout, P. B. *J. Phys. Chem.* **1995**, *99*, 11424. (b) Chen, Y.-M.; Armentrout, P. B. *J. Am. Chem. Soc.* **1995**, *117*, 9291. (c) Armentrout, P. B.; Chen, Y.-M. *J. Am. Soc. Mass Spectrom.* **1999**, *10*, 821. (d) Armentrout, P. B. *Organometallics* **2007**, *26*, 5486. (e) Michelini, M. C.; Rivalta, I.; Sicilia, E. *Theor. Chem. Acc.* **2008**, *120*, 395.

(14) (a) Armentrout, P. B. *Annu. Rev. Phys. Chem.* **1990**, *41*, 313. (b) Eller, K.; Schwarz, H. *Chem. Rev.* **1991**, *91*, 1121.

(15) See for instance: (a) Schröder, D.; Shaik, S.; Schwarz, H. *Acc. Chem. Res.* **2000**, *33*, 139. (b) Poli, R.; Harvey, J. N. *Chem. Soc. Rev.* **2003**, *32*, 1.

(16) (a) Becke, A. D. *J. Chem. Phys.* **1993**, *98*, 5648. (b) Lee, C.; Yang, W.; Parr, R. G. *Phys. Rev. B* **1988**, *37*, 785.

(17) (a) http://www.theochem.unistuttgart.de/pseudopotentiale/. (b) Küchle, W.; Dolg, M.; Stoll, H.; Preuss, H. *J. Chem. Phys.* **1994**, *100*, 7535.

(18) (a) Krishnan, R.; Binkley, J. S.; Seeger, R.; Pople, J. A. *J. Chem. Phys.* **1980**, *72*, 650. (b) Blaudeau, J.-P.; McGrath, M. P.; Curtiss, L. A.; Radom, L. *J. Chem. Phys.* **1997**, *107*, 5016. (c) Clark, T.; Chandrasekhar, J.; Schleyer, P. V. R. *J. Chem. Phys.* **1983**, *74*, 294.

(19) Frisch, M. J.; et al. *Gaussian 03.* See Supporting Information for full citation.

(20) (a) te Velde, G.; Bickelhaupt, F. M.; van Gisbergen, S. J. A.; Fonseca Guerra, C.; Baerends, E. J.; Snijders, J. G.; Ziegler, T. *J. Comput. Chem.* **2001**, *22*, 931. (b) Fonseca Guerra, C.; Snijders, J. G.; te Velde, G.; Baerends, E. J. *Theor. Chem. Acc.* **1998**, *99*, 391. (c) ADF2004.01, SCM, Theoretical Chemistry, Vrije Universiteit, Amsterdam, The Netherlands, http://www.scm.com.

(21) (a) Burke, K.; Perdew, J. P.; WangY. In *Electronic Density Functional Theory: Recent Progress and New Directions*; Dobson, J. F., Vignale, G., Das, M. P., Eds.; Plenum: New York, 1998. (b) Perdew, J. P. In *Electronic Structure of Solid′91*, Ziesche, P., Eschrig, H., Eds.; Akademie Verlag: Berlin, 1991; p 11. (c) Perdew, J. P.; Burke, K.; Wang, Y. *Phys. Rev. B* **1996**, *54*, 16533. (d) Perdew, J. P.; Chevary, J. A.; Vosko, S. A.; Jackson, K. A.; Pederson, M. R.; Singh, D. J.; Fiolhais, C. *Phys. Rev. B* **1992**, *46*, 6671. (e) Perdew, J. P.; Chevary, J. A.; Vosko, S. H.; Jackson, K. A.; Pederson, M. R.; Singh, D. J.; Fiolhais, C. *Phys. Rev. B* **1993**, *48*, 4978.

(22) Blaise, J.; Wyart, J.-F. Tables of Constants and Numerical Data. *International Tables of Selected Constants, Energy Levels and Atomic Spectra of Actinides*; 1992; Vol. 20, taken from http://www.lac.u-psud.fr/Database/Contents.html.

(23) Vallet, V.; Schimmelpfennig, B.; Maron, L.; Teichteil, C.; Leininger, T.; Gropen, O.; Grenthe, I.; Wahlgren, U. *Chem. Phys.* **1999**, *244*, 185.

JP9048154